Analysis of self-assembly of S-layer protein slp-B53 from Lysinibacillus sphaericus

European Biophysics Journal 46(2017)1, 77-89

DOI: https://doi.org/10.1007/s00249-016-1139-9

Analysis of self-assembly of S-layer protein slp-B53 from Lysinibacillus sphaericus

Jun Liu [1 2], Sven Falke [1], Bjoern Drobot [5], Dominik Oberthuer [1 3], Alexey Kikhney [4], Tobias Guenther [6], Karim Fahmy [5], Dmitri Svergun [4], Christian Betzel [1], Johannes Raff [5 6]

1 Laboratory for Structural Biology of Infection and Inflammation, Institute of Biochemistry and Molecular BiologyUniversity of Hamburg, Martin-Luther-King Platz, 620146 Hamburg, Germany
2 Bioengineering FacultySichuan University of Science and Engineering, Huixing Rd., Xueyuan Street 180 Zigong, 643000 Sichuan, China
3 Center for Free-Electron Laser Science (CFEL)DESYNotkestr. 8522607 Hamburg, Germany
4 European Molecular Biology Laboratory (EMBL)DESY Notkestr., 8522607 Hamburg, Germany
5 Institute of Resource EcologyHelmholtz-Zentrum Dresden-Rossendorf, Bautzner Landstr. 400, 01328 Dresden, Germany
6 Helmholtz Institute Freiberg for Resource Technology, Helmholtz-Zentrum Dresden-Rossendorf, Bautzner Landstr. 400, 01328Dresden, Germany

Abstract

The formation of stable and functional surface layers (S-layers) via self-assembly of surface-layer proteins on the cell surface is a dynamic and complex process. S-layers facilitate a number of important biological functions, e.g., providing protection and mediating selective exchange of molecules and thereby functioning as molecular sieves. Furthermore, S-layers selectively bind several metal ions including uranium, palladium, gold, and europium, some of them with high affinity. Most current research on surface layers focuses on investigating crystalline arrays of protein subunits in Archaea and bacteria. In this work, several complementary analytical techniques and methods have been applied to examine structure–function relationships and dynamics for assembly of S-layer protein slp-B53 from Lysinibacillus sphaericus: (1) The secondary structure of the S-layer protein was analyzed by circular dichroism spectroscopy; (2) Small-angle X-ray scattering was applied to gain insights into the three-dimensional structure in solution; (3) The interaction with bivalent cations was followed by differential scanning calorimetry; (4) The dynamics and time-dependent assembly of S-layers were followed by applying dynamic light scattering; (5) The two-dimensional structure of the paracrystalline S-layer lattice was examined by atomic force microscopy. The data obtained provide essential structural insights into the mechanism of S-layer self-assembly, particularly with respect to binding of bivalent cations, i.e., Mg^{2+} and Ca^{2+}. Furthermore, the results obtained highlight potential applications of S-layers in the fields of micromaterials and nanobiotechnology by providing engineered or individual symmetric thin protein layers, e.g., for protective, antimicrobial, or otherwise functionalized surfaces.

Keywords: Surface-layer protein, Self-assembly, Bivalent cations, AFM, DSC, SAXS

J. Liu and S. Falke contributed equally to this work.

Introduction

Surface layers (S-layers) are constituted of so-called surface-layer proteins (S-layer proteins) and have been intensively studied for more than six decades (Fagan and Fairweather 2014). In several studies it has been shown that bivalent cations interact with S-layer proteins (Word et al. 1983; Sleytr 1978; Koval and Murray 1984; Beveidge and Murray 1976); For example, Ca interacts not only in a nonspecific way, showing strong interaction with the protein backbone (Kummer et al. 2011), but also in a specific way, mediating lattice formation (Teixeira et al. 2010; Rad et al. 2015; Baranova et al. 2012). In general, S-layer proteins self-assemble to two-dimensional (2D) crystals (Györvary et al. 2003; Sára and Sleytr 2000; Sleytr et al. 1999; Pum et al. 1989; Sleytr 1975; Weinert et al. 2015), thereby providing the primary protective barrier for prokaryotic cells. S-layers can be regarded as the simplest protein membrane (Engelhardt 2007; Kern et al. 2011; Schuster and Sleytr 2009). For the 2D structure, different S-layer lattices with three types of space group symmetry have been found so far: oblique (p1, p2), square (p4), and hexagonal (p3, p6) (Fig. 1), where the morphological unit cell corresponds to one, two, four, and three or six identical (glyco)protein subunits, respectively (Sleytr et al. 1996).

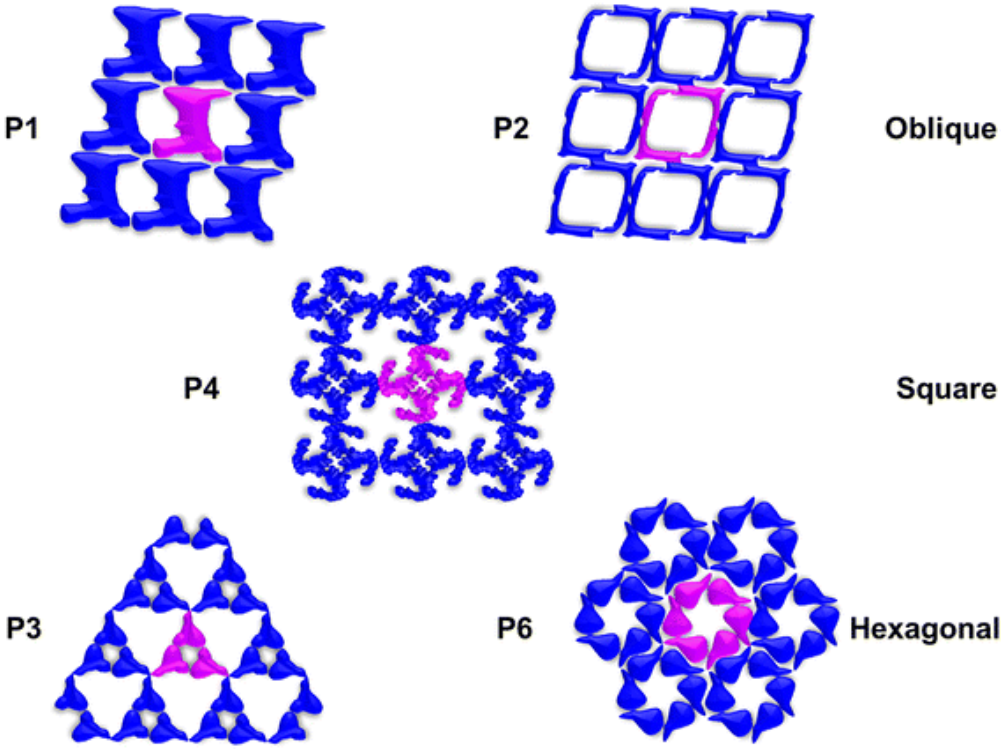

Fig. 1: Scheme of different types of S-layer symmetry (modified from Sleytr and Messner 1983). The parts edged in black represent one unit cell

Different S-layers are strongly suggested to be involved in cell-wall formation, selective cell protection, and regulation of cell-wall permeability (Peltier et al. 2011; Sockett 2009; Sara and Sleytr 1987). Furthermore, they are involved in the interaction between bacteria and their hosts, as well as with the outer environment. S-layers act as molecular sieves that mediate exchange of nutrients and metabolites (Horejs et al. 2011). In some pathogenic bacteria, S-layer proteins are also known to be key virulence factors (Kern and Schneewind 2010; Sabet et al. 2003; Dooley et al. 1988; Ishiguro et al. 1981; Kokka et al. 1990). They have potential applications in nanomedicine (Sleytr 1975; Glatter and Kratky 1982; Sleytr and Messner

1983; Sarkar 1996; Pollmann et al. 2005; Lipfert and Doniach 2007; Geisse 2009) and can act as a binding matrix for radioactive materials, e.g., for adsorption of uranium (Raff et al. 2003; Merroun et al. 2005). They are expected to be applicable to support cleanup and collection of nuclear pollution (Raff and Selenska-Pobell 2006). The self-assembly process of S-layer proteins has already been the subject of several studies, resulting in improved understanding (Rad et al. 2015; Chung et al. 2010; Shin et al. 2012), whereas little is known concerning the atomic structure of full-length S-layer proteins. So far, only the three-dimensional (3D) structure of the surface-layer protein SbsB from Geobacillus stearothermophilus (G. stearothermophilus) PV72/p2 has been published (Baranova et al. 2012) (PDB code 4aq1). However, to investigate potential applications, detailed information is required on the structure of S-layer proteins and their assembly (Horejs et al. 2011). There are two main reasons for this lack of structural information: (1) The fundamental building blocks of S-layers consist of proteins with high molecular weight (MW), ranging from 40 to 200 kDa (Sleytr and Messner 1983), which usually are either glycosylated or possess other posttranslational modifications. Therefore, it is not possible to analyze such structures using nuclear magnetic resonance (NMR) methods, which currently allow analysis of molecules up to approx. 30–40 kDa (Sarkar 1996). (2) Due to the fact that S-layers form functional 2D lattices rather directly by self-assembly, growth of the 3D crystals that would be required for X-ray crystallography is a huge challenge. S-layer proteins are evolutionarily optimized to form two-dimensional and not three-dimensional crystals. Thus, all attempts to identify and optimize conditions to obtain nucleation of ideal 3D crystals are constantly hindered by two-dimensional self-assembly. To solve the first full-length structure of an S-layer protein with atomic resolution, Baranova et al. (2012) used specific nanobodies to stabilize the S-layer protein SbsB from G. stearothermophilus. By applying this technique, crystals suitable for X-ray analysis could be obtained. The S-layer protein slp-B53 from Lysinibacillus sphaericus (Lederer et al. 2013) (L. sphaericus) consists of 1104 amino acids, including a 31-amino-acid signal peptide, and shows 30 % sequence identity with SbsB. To characterize slp-B53 and particularly the effect of cation binding and 2D self-assembly, a combination of five techniques, namely circular dichroism (CD) spectroscopy, atomic force microscopy (AFM), dynamic light scattering (DLS), small-angle X-ray scattering (SAXS), and differential scanning calorimetry (DSC), as well as additional structure predictions on the basis of sequence analysis were applied in this work.

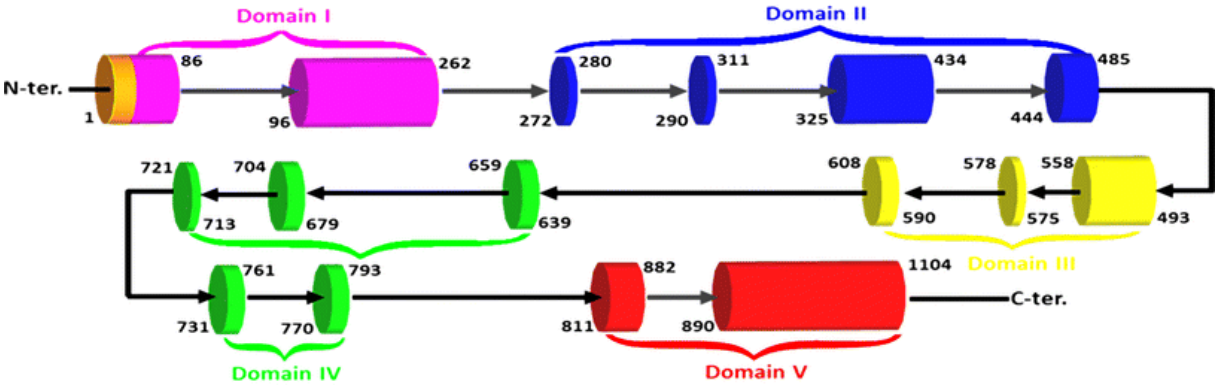

Fig. 2: Secondary structure as predicted by PredictProtein. Predicted flexible regions are summarized below; the topology diagram is artificially divided into five domains (or subdomains) displayed as colored columns. Flexible linkers, including disordered regions, are depicted as black arrows. Cylinders represent compactly folded regions. Lines with arrows indicate flexible or disordered regions. Domain I (pink) is most probably responsible for anchoring; domain II, shown in blue, domain III in yellow, domain IV, highlighted in green, as well as domain V in red were considered as self-assembly regions. The N-terminal signal peptide is shown in orange

Results and discussion

General characteristics and structure prediction

S-layer proteins are known to be highly flexible (Pavkov et al. 2008). Theoretical models (Fig. 2) as well as experimental data (CD spectroscopy, Fig. 4) were combined to obtain information about the secondary and tertiary structure, respectively, of the S-layer protein slp-B53.

As derived from its primary structure, the MW of slp-B53 is 116 kDa. Figure 2 displays the results obtained using PredictProtein (https://www.predictprotein.org/) to identify particularly potentially disordered regions of slp-B53. The results indicate that the region between amino acids 400 and 800 is highly flexible, in agreement with spectroscopic data presented below. The corresponding topology diagram is divided into five domains. Domain I, shown in pink, contains the SLH (S-layer homology) domain, which is responsible for anchoring. Domains II (blue), III (yellow), IV (green), and V (red) support self-assembly. The signal peptide is colored orange. Furthermore, the results allow one to propose a shape for the S-layer protein, consisting of functionally important domains, shown in Fig. 3. I-TASSER succeeded in generating a valuable model of slp-B53 by homology modeling procedures (Roy et al. 2010, 2012; Zhang 2008) (C score = −1.10, TM score = 0.58 ± 0.14). Homolog PDB models were used, including the structures of SbsB (PDB code 4aq1) from G. stearothermophilus (Sleytr and Messner 1983) and an SLH domain (PDB code 3pyw) from Bacillus anthracis, representing a characteristic domain of S-layer proteins sharing sequence homology of 22 % with slp-B53. This domain contains a three-helix bundle at the spindle base and a single α-helix. The connecting loops generate the three prongs (Kern et al. 2011). The modeled structure shows the presence of several flexible domains (see also Fig. 5d).

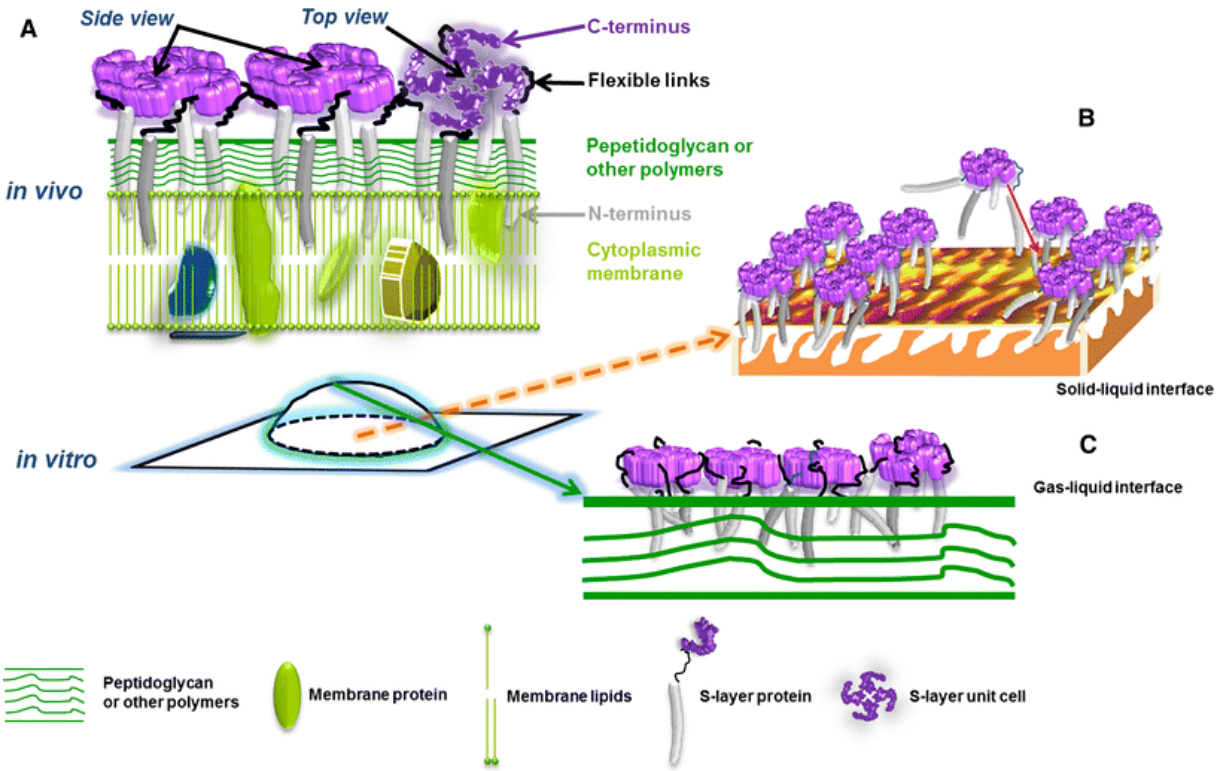

Fig. 3: Scheme indicating the shape of S-layer self-assembly. a Shape of S-layer self-assembly scheme in vivo. b Mimic formation diagram of S-layer at solid–liquid interface. c Analog diagram displaying the formation of S-layers in solution

Secondary-structure analysis by CD spectroscopy

Initially, CD spectroscopy data verified that the purified protein is well folded (Fig. 4). Moreover, they revealed that the percentage of α-helical and β-sheet structures remained almost constant upon addition of cations, independent of the choice from a set of algorithms provided by DICHROWEB (Table 1).

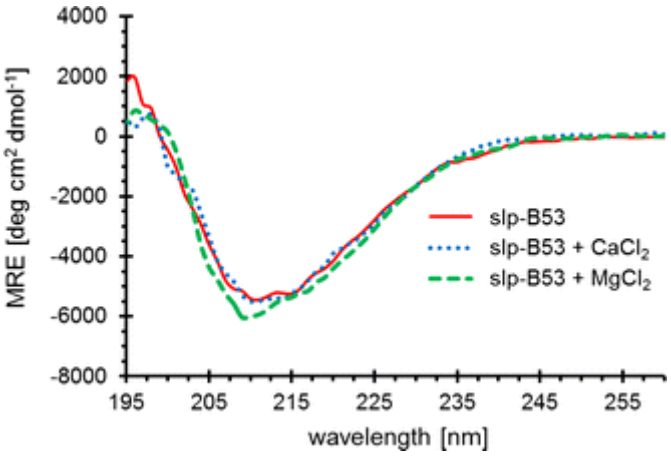

Fig. 4: Secondary-structure content of slp-B53 as revealed by far-ultraviolet (UV) CD spectroscopy. The solid red curve represents the spectrum of slp-B53 without bivalent cations; the dotted curve is the averaged spectrum upon addition of Ca^{2+}; the dashed curve displays the averaged spectrum of slp-B53 upon supplementation with Mg^{2+}

Sample	Algorithm	NRMSD	α-Helix (%)	β-Sheet (%)	Regions with low structural complexity (%)
slp-B53	Selcon3	0.451	35	11	54
	CCSSTR	–	53	23	24
	Contin-LL	0.190	61	6	33
	Mean value	–	50	13	37
slp-B53 + $CaCl_2$	Selcon3	0.504	35	12	55
	CCSSTR	–	46	26	28
	Contin-LL	0.239	59	4	37
	Mean value	–	47	14	40
slp-B53 + $MgCl_2$	Selcon3	0.484	34	11	55
	CCSSTR	–	56	19	26
	Contin-LL	0.208	62	2	36
	Mean value	–	51	11	39

Table 1: Secondary-structure evaluation of slp-B53 by CD spectroscopy

For all samples, the relative β-sheet content was comparatively low according to the detailed structure evaluation. Similar to the percentage of α-helix, disordered regions account for almost half of the full-length slp-B53, which may indicate structural flexibility. The CD results confirmed that addition of bivalent cations did not have a significant effect on the secondary structure of the domains. This does not exclude changes in tertiary structure, because unstructured regions may allow repositioning of secondary-structure elements with respect to each other. This would not affect the secondary-structure content and would thus leave the CD spectrum unchanged. Moreover, the CD spectroscopy results resemble the structure that was modeled in silico. The fractions of secondary structure, as determined either experimentally by CD spectroscopy or by in silico data resulting from the above-mentioned two modeling servers, support partial flexibility of slp-B53 in solution.

Analysis of SAXS data

The oligomeric state and tertiary structure of slp-B53 in solution in the absence and presence of bivalent cations were analyzed using SAXS (Fig. 5). The radius of gyration R_g and the maximum dimension D_{max} obtained from the data collected in the absence of cations were 5.8 ± 0.4 and 22 ± 2 nm, respectively; along with the Kratky plot (Fig. 5b), these values suggest a folded but extended structure. A tentative ab initio model of the protein (Fig. 5d) displays an extended multidomain shape, in agreement with this expectation. The MW of 166 ± 17 kDa is somewhat larger than the expected monomer MW (116 kDa) and indicates that some oligomers are present in solution along with monomers. The data collected in the

presence of cations are similar overall and within the experimental error range for values of R_g, D_{max}, and MW (Table 2).

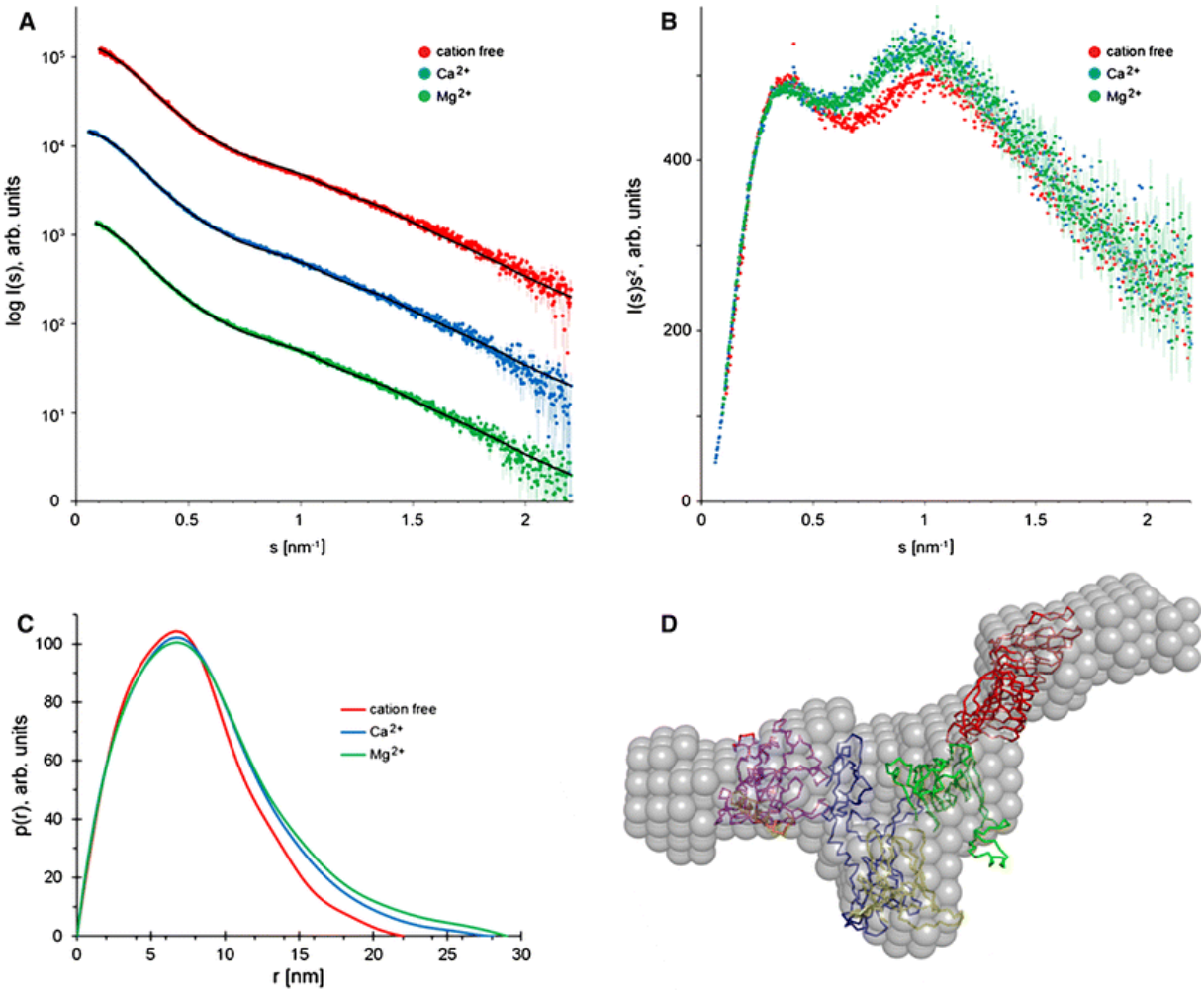

Fig. 5: SAXS analysis and modeling of slp-B53. a Processed solution scattering patterns of slp-B53 without cations (red), and with Ca^{2+} (blue) and Mg^{2+} (green) fit by SASREFMX as a mixture of monomers and dimers (black lines). Logarithm of X-ray scattering intensity I(s) in arbitrary units is plotted versus the modulus of the scattering vector s in inverse nanometers. Curves are displaced vertically for clarity. b Kratky plot of experimental data, i.e., $I(s)s^2$ versus s; here the difference between cation-free slp-B53 (red) and slp-B53 with Ca^{2+} (blue)/Mg^{2+} (green) is most pronounced around s = 0.8 nm^{-1}. c Corresponding pair-distance distribution functions p(r). d Ab initio dummy atom model of cation-free slp-B53 (grey spheres) superposed with the monomer rigid-body model consisting of all five putative (color-coded) domains, including the N-terminal signal peptide

Data collection parameters			
Instrument	EMBL beamline P12 (Zhang 2008)		
Wavelength (nm)	0.124		
s-Range (nm^{-1})	0.03–4.8		
Exposure time (s)	0.05 × 20		
Concentration range (mg mL^{-1})	1.0–7.5		
Temperature (K)	283		
Structural parameters	slp-B53	With Ca^{2+}	With Mg^{2+}
R_g (nm) (from Guinier)	5.8 ± 0.4	6.4 ± 0.7	6.6 ± 0.6
R_g (nm) [from p(r)]	6.1 ± 0.6	6.8 ± 0.7	7.3 ± 0.7
D_{max} (nm)	22.0 ± 2.2	28.1 ± 2.8	29.0 ± 2.9
Molecular weight determination			
MW (kDa) from DAMMIF volume	166 ± 17	222 ± 22	178 ± 18
Calculated MW (kDa) from sequence	116	116	116
Monomer:dimer volume fractions	0.7:0.3	0.6:0.4	0.6:0.4
Software employed			
Primary data reduction and processing	SASFLOW pipeline (Franke et al. 2012)		
Ab initio analysis	DAMMIF (Franke and Svergun 2009)		
Rigid-body modeling	SASREFMX (Petoukhov et al. 2012)		

Table 2: SAXS data collection and analysis parameters

Using rigid-body modeling, it was still possible to fit the three experimental datasets (Fig. 5a) by a mixture of monomeric protein constructed from the individual domains, accounting for possible dimerization effects. In the absence of cations, the ratio of monomers to dimers turned out to be 0.7:0.3 by volume; after addition of either of the cations, the amount of dimers increased to approximately 0.4. The rigid-body model of the monomer is compatible with the ab initio model in overall appearance (Fig. 5d); here, the nonfilled protrusion in the ab initio shape can be attributed to partial dimerization via hydrophobic interactions.

Thermal stability of slp-B53 is controlled by bivalent cations

Figure 6 shows the results of DSC performed with slp-B53 under different ionic conditions. Four Gaussian curves describe the heat-capacity changes during thermal unfolding in all cases. The first unfolding transition at about 45 °C accounted for 13–20 % of the total integrated heat uptake. We assign it to a varying fraction of destabilized slp-B53 (F1) in each sample, because its DSC curve extended over a wide temperature interval. The second (F2) and third (F3) components represent states with increasing stability, which were assigned to breakage of protein domains or intermolecular contacts that are not dominated by hydrophobic interactions, as suggested by the lack of heat-capacity changes upon unfolding (see below). These proteins denature in the desalted sample at 51 and 53 °C, respectively. Finally, the most stable protein fraction (S) unfolded at about 60 °C, which under all conditions was accompanied by an increase of the posttransition heat capacity that was not present for the other fractions. Such an increase is typical of exposure of hydrophobic protein

surfaces during unfolding (Makhatadze and Privalov 1995; Prabhu and Sharp 2005; Privalov and Gill 1988) and was accounted for by a sigmoidal function with variable position, steepness, and amplitude in the fits.

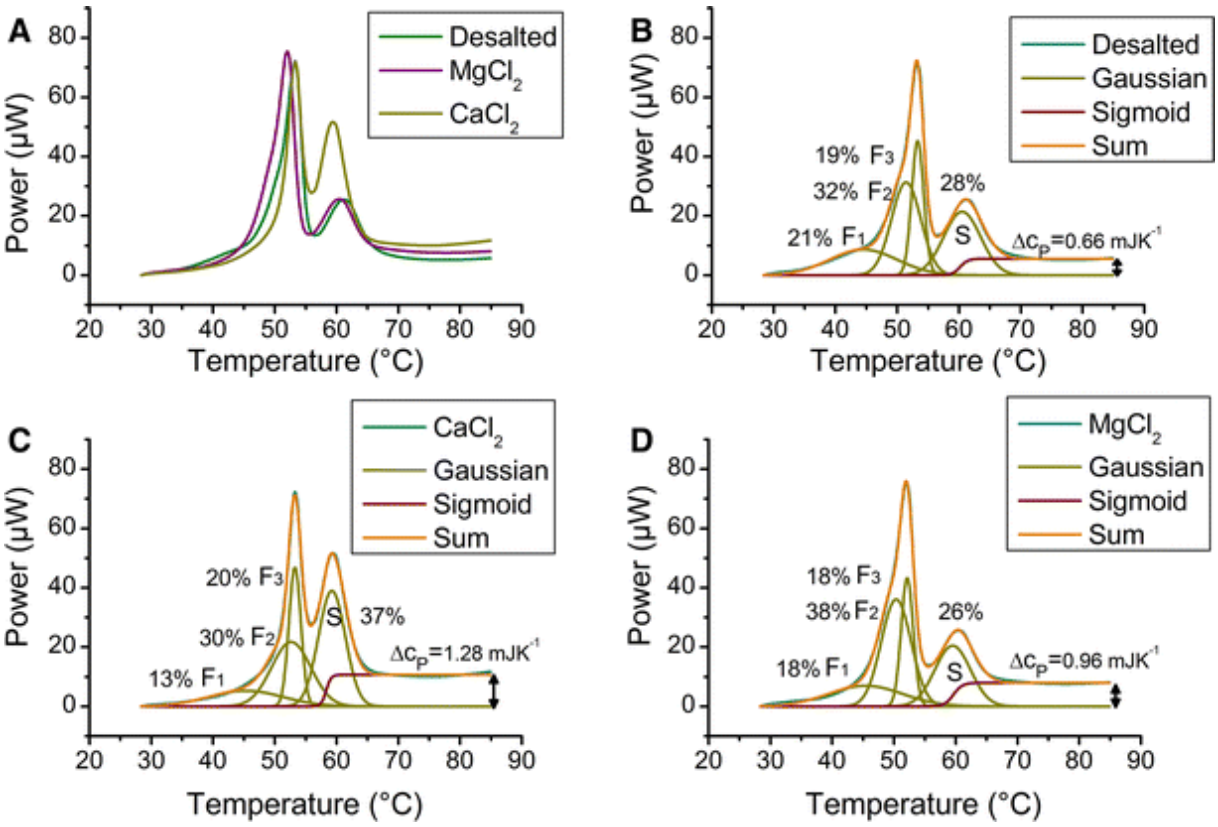

Fig. 6: Cation dependency of DSC curves of thermal unfolding of slp-B53. a DSC curves in the absence and presence of the indicated ions (10 mM). b–d Raw data (as in a) with fit Gaussian DSC components assigned to fractions with low stability (F1–F3) and the most stable, S-layer-like state (S), with their respective percentage fractions of the total heat of unfolding. The S fraction grows upon Ca^{2+} binding at the expense of the least stable fraction F1. The sigmoidal function accounts for the plotted changes in heat capacity Δc_p and is a characteristic feature of the S state

The most stable fraction S also exhibited the strongest modulation by ions. Its contribution to the DSC signal rose from less than 28 % in the absence of salts to more than 36 % in the presence of calcium. In agreement with the lattice-stabilizing function of calcium and with the increasing size of protein assemblies in the presence of Ca^{2+} observed by DLS (see below), we assign the high-temperature transition to thermal breakage of intermolecular protein–protein contacts, as would be expected upon denaturation of the S-layer lattice. The concomitant decrease of the F1 fraction suggests that calcium recruits the least stable domains for extension of the highly stable, S-layer-like protein assembly. In contrast, the enthalpic contributions from the F2 and F3 states, which are of intermediate stability, remained almost constant. Magnesium was much less effective in evoking the formation of the S fraction, again in agreement with the lack of larger protein assemblies (according to DLS) and the smaller heat-capacity change during unfolding of the S state in the presence of Mg^{2+}. The assignment of the 60 °C transition to unfolding of an S-layer-like lattice is further supported by the width of the thermal transition, which decreased from 7 to 5 °C in the desalted and

calcium-bound state, respectively. This indicates that the unfolding becomes cooperative, as expected for a paracrystalline lattice.
Whereas the S fraction can be attributed to an S-layer-like lattice with hydrophobic intermolecular contacts in the presence of Ca^{2+}, the assignment of the other fractions is ambiguous. They may represent different degrees of oligomerization, but could also be caused by unfolding of individual protein domains of monomeric slp-B53. In particular, the structures that cause the F3 peak show a thermal signature that is entirely independent of the presence of cations. Therefore, we tentatively assign this fraction to unfolding of a protein domain that is involved neither in ion binding nor in lattice formation. In contrast, the formation of the S-layer-like S state by Ca^{2+} is clearly dependent on depleting the fractions that give rise to the F1 and F2 peaks.
In summary, neutralization of carboxy groups on the protein surface by calcium is probably crucial for reducing protein solubility and increasing packing into the S-layer by abolishing electrostatic repulsion. The data support a model in which calcium but not magnesium promotes S-layer formation by assembling monomers into a lattice that is largely held together by hydrophobic contacts. The increase of the solvent-exposed hydrophobic surface during unfolding was thus largest for Ca^{2+}-bound S-layers, where the hydrophobic intermolecular contacts were initially buried in the protein interfaces of the lattice and became exposed only upon thermal denaturation. Correspondingly, the steepness and amplitude of the sigmoidal curve scaled with the fraction S. In the absence of ions or with magnesium, F1 and F3 states dominated. These states showed no increase in hydrophobic exposure during denaturation. The least stable, F1 fraction decreased the most upon Ca^{2+}-induced lattice formation and is thus mostly involved in the ion-dependent formation of the much more stable tertiary and quaternary structure in the S state.

DLS experiments

DLS was used to assess particularly the size and oligomerization of slp-B53 in appropriate buffer solutions before and after addition of bivalent cations. A monodisperse solution of monomeric protein characterized by an R_H of 4.9 ± 1.1 nm, which corresponds to an approximate MW of 120 kDa, was obtained by initial ultracentrifugation before adding cations. This approximation well indicates a monomeric state. The DLS data showed that, after 24 h, a mixture of small oligomers peaking at an R_H of 7.9 ± 0.8 nm was present in the cation-free solution. However, after addition of 10 mM $CaCl_2$, the distinct increase of R_H to 7–25 nm indicated formation of relatively large slp-B53 oligomers along with a few even larger oligomers with R_H > 100 nm after 24 h. In contrast, after adding Mg^{2+}, DLS experiments showed that the hydrodynamic radius of monomeric slp-B53 remained stable within the same timeframe, with an indication of some dimers in the sample (Fig. 7).

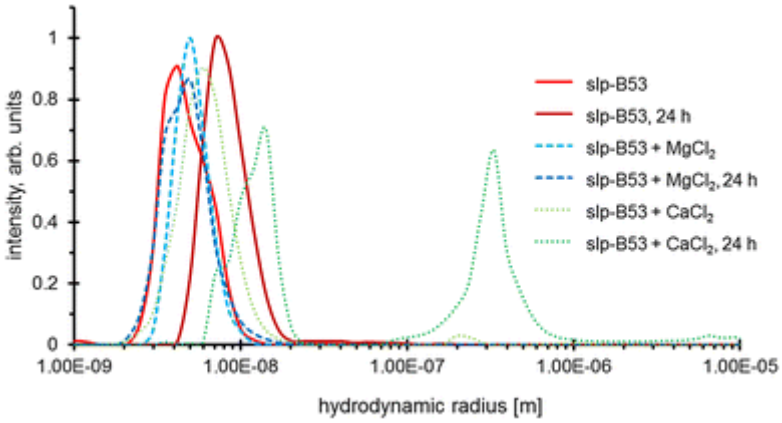

Fig. 7: Size distribution analysis of slp-B53 in solution via dynamic light scattering at different time points reveals specific induction of oligomer assembly upon addition of $CaCl_2$. For comparison, the results for a solution without cations in pure water are displayed. Prior to ultracentrifugation, slp-B53 solution contained additional oligomeric particles (data not shown) beside the putative monomeric state with R_H of 4.9 ± 1.1 nm (red)

Formation of S-layer analyzed by AFM

As summarized above, S-layer proteins have the ability to self-assemble, forming distinct crystalline lattices. AFM experiments provided data regarding slp-B53 self-assembly and symmetry, as shown in Fig. 8, revealing p4 symmetry.

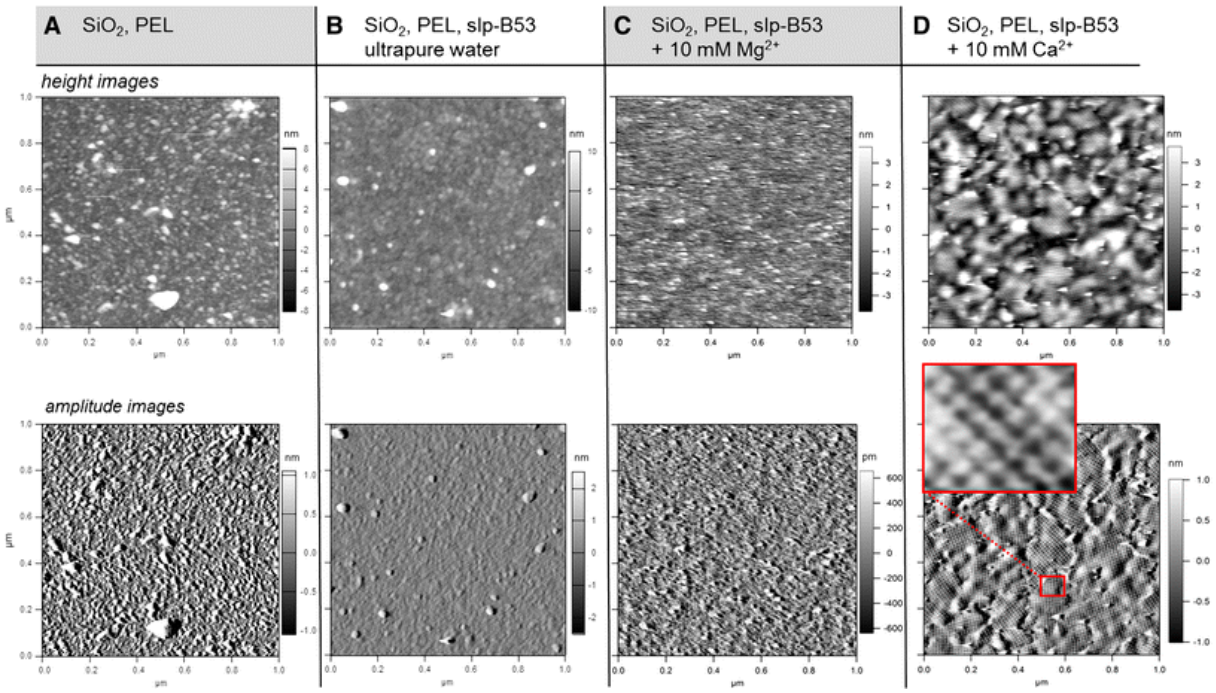

Fig. 8: AFM investigations of 2D crystallization of slp-B53 (1 × 1 μm^2). a Serves as blank control (without protein), comprising only SiO_2 (silica wafer) and polyelectrolyte layers (PEL); b–d show scanning pictures of tested polyelectrolyte-supported protein samples of SiO_2 + PEL + slp-B53 in ultrapure water, SiO_2 + PEL + slp-B53 + 10 mM Mg^{2+}, and SiO_2 + PEL + slp-B53 + 10 mM Ca^{2+}, respectively. Upper images display the height trace, while lower images record the amplitude trace (pseudo 3D). The inset in d shows a selected magnification

There was no significant difference between the blank control (SiO_2 + PEL) and test samples (SiO_2 + PEL + slp-B53) in ultrapure water and in solution containing 10 mM $MgCl_2$. The slight blurring for the sample with slp-B53 can be explained by contamination of the cantilever. It is very likely that slp-B53 is nonspecifically adsorbed onto the probe surface and the polyelectrolyte-covered SiO_2 support. Also, no crystalline (2D) structures or any type of symmetry could be recognized in these conditions (Fig. 8a–c). On the other hand, a tetragonal S-layer conformation was observed in the presence of 10 mM $CaCl_2$ at pH 7.4. It consisted of four single elongated slp-B53 molecules displaying p4 symmetry, as deduced from Fig. 8d. An elongated shape of the S-layer protomers well reflects the structural parameters obtained by SAXS. The unit cell has a dimension of 12.9 ± 0.9 nm.

Combining the results of in silico modeling and AFM experiments, the formation of S-layers in vivo can be interpreted as shown in Fig. 3. One domain comprises the positively charged N-terminus that binds to the negatively charged secondary cell-wall polymer and thus is responsible for anchoring. Another functionally important domain is located at the C-terminus. The C-terminal domain interacts with the counterparts of the neighboring S-layer protein, thus forming the S-layers. These two domains are interconnected by flexible linkers. The highly adaptable linker domains explain why S-layer proteins are highly flexible, can adapt their conformations, and allow interaction with surrounding S-layer proteins to form a stable symmetric 2D S-layer structure. Based on the AFM results, it can be assumed that S-layer proteins first adsorb at interfaces in a defined orientation, followed by addition of further protein monomers and formation of latticed S-layer sheets, as implied in Fig. 3b, c.

As indicated by previous results, S-layer proteins from the closely related L. sphaericus strain JG-A12 possess one to two Mg^{2+}-binding sites and about ten Ca^{2+}-binding sites, as confirmed by inductively coupled plasma mass spectroscopy (ICP–MS) measurements. It can be assumed that uptake of Mg^{2+} instead of Ca^{2+} induces conformational interdomain changes with buried self-assembly sites (Fig. 9). Instead of forming stable, almost monodisperse slp-B53 molecules in solution, as observed upon interaction with Mg^{2+}, uptake and binding of Ca^{2+} results in exposure of the self-assembly sites. This slight rearrangement of the tertiary structure allows intermolecular interaction between S-layer proteins, leading to native 2D lattices with average-sized crystallites.

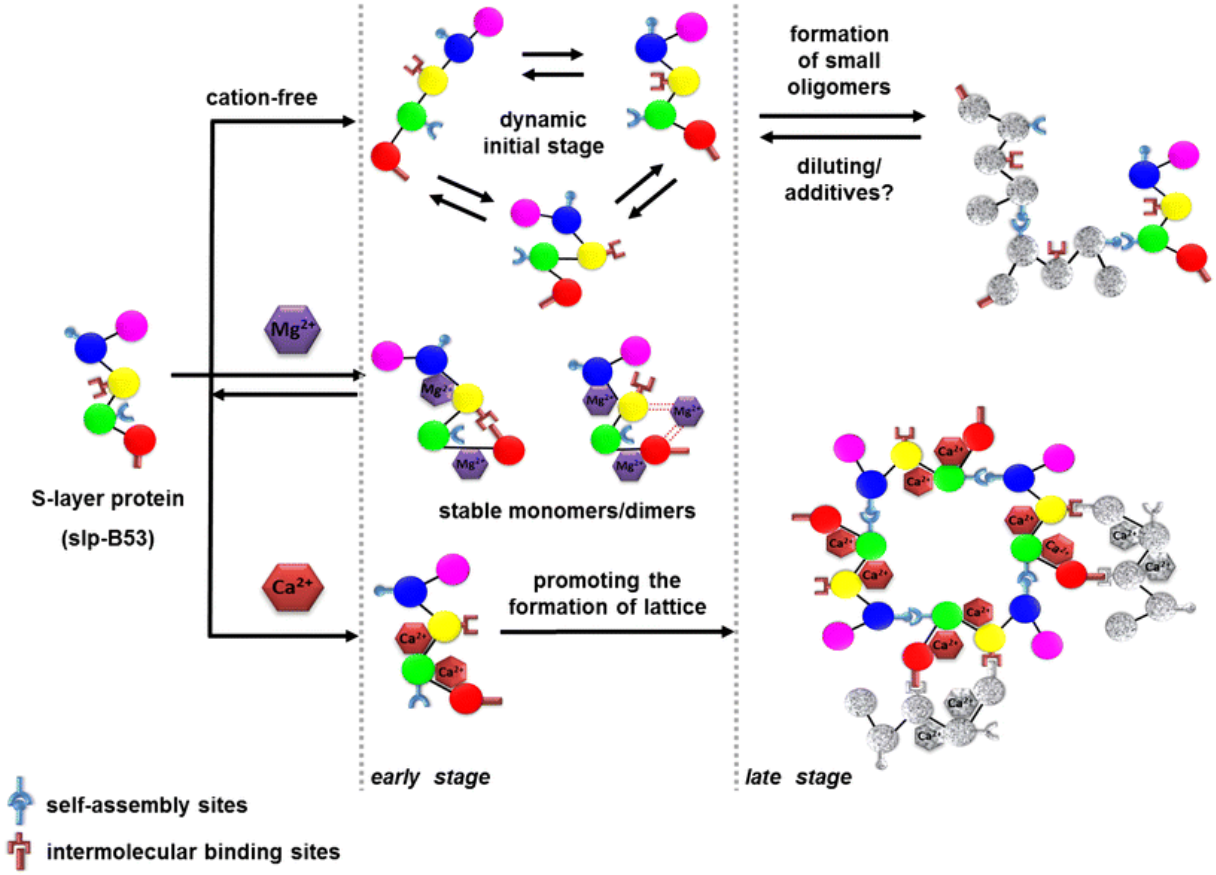

Fig. 9: Influence of bivalent cations on S-layer protein assembly

The AFM and DLS results in combination with those from DSC and SAXS support the understanding that ubiquitous bivalent cations, e.g., Ca^{2+}, have a substantial influence on the structural requirements of the S-layer protein assembly. Nonetheless, the secondary structure involving some regions of low structural complexity is widely conserved with a highly similar tertiary structure after addition of selected cations.
Obviously, addition of Mg^{2+} helps to maintain the monodispersity of slp-B53, thus supporting crystallization experiments (Borgstahl 2007). Addition of Ca^{2+} promotes formation of large 2D lattices, as previously discussed and visualized in Fig. 9.

Experimental

slp-B53 was prepared as described in detail before (Raff et al. 2003). Lyophilized protein was solved in 6 M guanidine hydrochloride. Ion-free solutions were produced by desalting via a HiTrap column. Remaining aggregates were removed by centrifugation at 50,000×g. The MW of slp-B53 is 116 kDa [as derived from its sequence and sodium dodecyl sulfate (SDS) polyacrylamide gel electrophoresis (PAGE)]. Protein concentrations were determined by absorption spectroscopy at 280 nm using a Nanodrop 2000c (PEQLAB Biotechnologie, Erlangen, Germany). The influence of bivalent cations was assessed using solutions of $MgCl_2$ (Carl Roth, Karlsruhe, Germany) as well as $CaCl_2$ (Merck, Darmstadt, Germany) dissolved in pure water. The respective protein solutions were preincubated with either bivalent cation for at least 5 min prior to DLS and SAXS data collection and for 2 or 24 h for CD, DSC, and further DLS measurements.

Prediction of disordered regions of S-layer proteins was carried out by using the PredictProtein server (Rost et al. 2004). Homology modeling of the tertiary structure and further characterization of the protein were carried out with the web server I-TASSER (Roy et al. 2010, 2012; Zhang 2008). Secondary structures of slp-B53 (0.05 mg mL^{-1}) in the presence/absence of different cations (10 mM each) were investigated by CD spectroscopy. A JASCO J-815 instrument (JASCO Germany GmbH, Gross-Umstadt, Germany) was applied along with a 1-mm quartz cuvette at 20 °C. Evaluation of measurements and prediction of the secondary structures was carried out by using the Selcon3/CDSSTR/Contin-LL algorithm of DICHROWEB (Whitmore and Wallace 2008) hosted at Birkbeck College (University of London, UK). AFM allows investigation of the shape of biological macromolecules as well as examination of surface characteristics (Geisse 2009). An AFM system (MFP-3D-Bio, Asylum Research, Santa Barbara, CA, USA) was applied to reveal details of the self-assembly phenomenon and the lattice type of the S-layer. All measurements were performed in the respective solution using a closed fluid cell (Asylum Research, Santa Barbara, CA, USA) to prevent drying artifacts. For AFM measurements, the dynamic, alternating-current (AC) mode of the instrument and a cantilever with spring constant <0.1 N m^{-1} were used. Therefore, a BioLever mini (BL-AC40TS-C2) was applied. As support for S-layers, polyelectrolyte coatings [substrate, silica wafer SiO_2 + polyelectrolyte layer composed of three alternating layers of polyethyleneimine (MW 25,000, Sigma), polystyrenesulfonate (MW 70,000, Sigma), and polyethyleneimine, PEL coating with slp-B53 (approx. 0.2 mg mL^{-1})] were produced as described before (Georgieva et al. 2004; Balkundi et al. 2009; Franz et al. 2010).

The dispersity and radius distribution of slp-B53 (3 mg mL^{-1}) with and without addition of bivalent cations, such as Ca^{2+} and Mg^{2+} at concentration of 10 mM, were determined by DLS. The DLS system (SPECTROLIGHT™ 600, Xtal Concepts, Hamburg, Germany) was also used to monitor self-assembly in a corresponding 3 mg mL^{-1} solution after addition of different bivalent cations in situ (Dierks et al. 2008). All DLS measurements were carried out at room temperature and evaluated using the provided software.
Synchrotron-radiation small-angle X-ray scattering data from four solute concentrations of slp-B53 ranging from 1 to 7 mg mL^{-1} in pure water and immediately after addition of 10 mM $MgCl_2$ or 10 mM $CaCl_2$, respectively, were collected at EMBL beamline P12 at storage ring PETRA III (DESY, Hamburg, Germany) (Blanchet et al. 2012). Data were collected using a 2D photon-counting Pilatus 2M pixel detector (Dectris) at sample–detector distance of 3.0 m and wavelength of $\lambda = 0.124$ nm, covering the momentum transfer range of $0.03\ nm^{-1} < s < 4.8\ nm^{-1}$ ($s = 4\pi \sin\theta/\lambda$, where 2θ is the scattering angle). To monitor for radiation damage, 20 successive 50-ms exposures of protein solutions were compared, and no significant changes were observed. Data were normalized to the intensity of the transmitted beam and radially averaged. The scattering of the buffer was subtracted, and the difference curves were scaled for protein concentration. The low-angle data measured at lower protein concentrations were extrapolated to infinite dilution and merged with the higher-concentration data to yield the final composite scattering curves. The radius of gyration R_g along with the particle pair-distance distribution function p(r) and maximum dimension D_{max} were computed by the automated SAXS data analysis pipeline SASFLOW (Franke et al. 2012). The composite scattering curves were used to generate low-resolution ab initio shapes of each protein using the program DAMMIF (Franke and Svergun 2009). This program uses an assembly of densely packed beads to represent the particle shape and employs simulated annealing to construct a compact interconnected model that fits the experimental I(s) data. Ten DAMMIF runs were performed to check solution stability, resulting in well-superimposable models. Given the uncertainty in determining the protein concentration, it was difficult to estimate the MW of the solute from the forward scattering. The excluded volume reported by DAMMIF was used to evaluate the MW, assuming that the protein volumes in

nm^3 are about two times the MWs in kDa. Rigid-body modeling was performed using the program SASREFMX (Petoukhov et al. 2012). Given the signal peptide and five individual domains (domain I–V) cut from an slp-B53 homology model, the scattering amplitudes were precomputed by the program CRYSOL (Svergun et al. 1995). Starting from the tentative model, SASREFMX used simulated annealing to search for a nonoverlapping interconnected configuration of domains fitting the three experimental data as a monomer:dimer mixture; the momentum transfer range of $0.1\ nm^{-1} < s < 2.2\ nm^{-1}$ was taken into account. The overall parameters evaluated from SAXS data are summarized in Table 2. The scattering data and models were deposited in SASBDB (Valentini et al. 2015) with codes SASDA49 (cation free), SASDA59 (with Ca^{2+}), and SASDA69 (with Mg^{2+}).
DSC measurements were carried out on a nano-DSC (TA Instruments, Eschborn, Germany). A concentration of 7.5 mg mL^{-1} slp-B53 was used in all experiments; the heating rate was 0.5 K min^{-1}. Cation concentrations were 10 mM for runs with $CaCl_2$ and $MgCl_2$, respectively. Unfolding curves were fit in MATLAB R2015a (using the Optimization Toolbox) by Gaussian components and a sigmoidal curve to quantify the contributions from different protein fractions and posttransition heat-capacity changes, respectively. Refolding was not observed in reverse temperature runs.

Conclusions

S-layer proteins represent an interesting model system for studying self-assembly processes at molecular level. In this study, it was shown that the secondary structure of slp-B53 contains a substantial amount of turns, loops, and disordered regions. The α-helix/β-sheet content was not significantly altered upon addition of bivalent cations. The S-layer proteins from L. sphaericus build a basic assembly form with p4 symmetry (Fig. 8). The overall structure of slp-B53 from L. sphaericus was analyzed and modeled (Fig. 5). It is well accepted that S-layer proteins are prone to bind bivalent cations whenever these are added in solution. Here, we demonstrated that addition of Mg^{2+} prevents self-assembly and enhances the monodispersity of S-layer protein slp-B53. However, addition of Ca^{2+} supports a defined oligomerization process with regular 2D lattice formation of slp-B53. Experimental SAXS analysis showed that the molecular shape of slp-B53 is elongated, containing several small domains that are probably flexibly interconnected, allowing variability of the tertiary structure. Even though the shape is only slightly altered in the presence of bound cations, DSC confirmed that bivalent cations significantly influence the thermal stability. Moreover, the structural influence of common bivalent cations on slp-B53 is indicated to be critical for the ratio of oligomers according to DLS and SAXS results. Additional information could also be obtained by anomalous SAXS (ASAXS) utilizing scattering signals in the vicinity of Ca or Mg absorption edges. Such ASAXS experiments would provide information about the distribution of the bound cations in the protein. Such studies will require homogeneous solutions of proteins with tightly bound cations in the absence of free cations in solution. A relatively high degree of flexibility indicated by CD spectroscopy was taken into consideration to obtain a stretched rigid-body model (Fig. 5d) of the monomeric protein from the individual domains as modeled in silico. This model is in good agreement with the independently calculated ab initio shape. Overall, the combination of CD spectroscopy, AFM, DLS, DSC, and SAXS results also demonstrates complementarily why it is rather difficult or even impossible to obtain 3D crystals suitable for X-ray analysis. Not only is 2D crystallization evolutionarily favored over 3D crystallization, but the high content of regions lacking secondary-structure elements as well as the rather elongated multidomain structure of slp-B53 facilitate intermolecular flexibility. A regulatory mechanism for the assembly of a selected typical S-layer protein is proposed.

Acknowledgments The work was supported by grants from the BMBF Röntgen–Ångström Cluster Project (RAC) under project number 05K12GU3 and by the DFG–Excellence Cluster CUI (Centre for Ultra-Fast Imaging), from CNPq, Brazil under project number 33.654.831/1001-36. Jun Liu was assisted by the China Scholarship Council (CSC) via Grant No. 2010629147 and by the Technology Foundation for Selected Overseas Chinese Scholar, Ministry of Personnel of China. Sven Falke, Christian Betzel, and Dmitri Svergun further acknowledge support from a BMBF grant, referring to project number 05K13GU2.

References

Balkundi SS, Veerabadran NG, Eby DM, Johnson GR, Lvov YM (2009) Encapsulation of bacterial spores in nanoorganized polyelectrolyte shells. Langmuir 25:14011–14016

Baranova E, Fronzes R, Garcia-Pino A, Van Gerven N, Papapostolou D, Péhau-Arnaudet G, Pardon E, Steyaert J, Howorka S, Remaut H (2012) SbsB structure and lattice reconstruction unveil Ca^{2+} triggered S-layer assembly. Nature 487(7405):119–122

Beveidge T, Murray R (1976) Dependence of the superficial layers of Spirillum putridiconchylium on Ca^{2+} or Sr^{2+}. Can J Microbiol 22:1233–1244

Blanchet CE, Zozulya AV, Kikhney AG, Franke D, Konarev PV, Shang W, Klaering R, Robrahn B, Hermes C, Cipriani F (2012) Instrumental setup for high-throughput small- and wide-angle solution scattering at the X33 beamline of EMBL Hamburg. J Appl Crystallogr 45:489–495

Borgstahl GE (2007) How to use dynamic light scattering to improve the likelihood of growing macromolecular crystals. In: Macromolecular crystallography protocols. Springer, Berlin, pp 109–130

Chung S, Shin S, Bertozzi C, De Yoreo J (2010) Self-catalyzed growth of S layers via an amorphous-to-crystalline transition limited by folding kinetics. PNAS 107:16536–16541
Dierks K, Meyer A, Einspahr H, Betzel C (2008) Dynamic light scattering in protein crystallization droplets: adaptations for analysis and optimization of crystallization processes. Cryst Growth Des 8:1628–1634

Dooley J, McCubbin W, Kay C, Trust T (1988) Isolation and biochemical characterization of the S-layer protein from a pathogenic Aeromonas hydrophila strain. J Bacteriol 170:2631–2638

Engelhardt H (2007) Are S-layers exoskeletons? The basic function of protein surface layers revisited. J Struct Biol 160:115–124

Fagan R, Fairweather N (2014) Biogenesis and functions of bacterial S-layers. Nat Rev Microbiol 12:211–222

Franke D, Svergun DI (2009) DAMMIF, a program for rapid ab initio shape determination in small-angle scattering. J Appl Crystallogr 42:342–346

Franke D, Kikhney AG, Svergun DI (2012) Automated acquisition and analysis of small angle X-ray scattering data. Nucl Instrum Methods Phys Res Sect A 689:52–59

Franz B, Balkundi SS, Dahl C, Lvov YM, Prange A (2010) Layer-by-layer nano-encapsulation of microbes: controlled cell surface modification and investigation of substrate uptake in bacteria. Macromol Biosci 10:164–172

Geisse NA (2009) AFM and combined optical techniques. Mater Today 12:40–45
Georgieva R, Moya S, Donath E, Bäumler H (2004) Permeability and conductivity of red blood cell templated polyelectrolyte capsules coated with supplementary layers. Langmuir 20:1895–1900

Glatter O, Kratky O (1982) Small angle X-ray scattering. Academic, London
Györvary ES, Stein O, Pum D, Sleytr UB (2003) Self-assembly and recrystallization of bacterial S-layer proteins at silicon supports imaged in real time by atomic force microscopy. J Microsc 212:300–306

Horejs C, Gollner H, Pum D, Sleytr UB, Peterlik H, Jungbauer A, Tscheliessnig R (2011) Atomistic structure of monomolecular surface layer self-assemblies: toward functionalized nanostructures. ACS Nano 5:2288–2297

Ishiguro E, Kay W, Ainsworth T, Chamberlain J, Austen R, Buckley J, Trust T (1981) Loss of virulence during culture of Aeromonas salmonicida at high temperature. J Bacteriol 148:333–340

Kern J, Schneewind O (2010) BslA, the S-layer adhesin of B. anthracis, is a virulence factor for anthrax pathogenesis. Mol Microbiol 75:324–332

Kern J, Wilton R, Zhang R, Binkowski TA, Joachimiak A, Schneewind O (2011) Structure of surface layer homology (SLH) domains from Bacillus anthracis surface array protein. J Biol Chem 286:26042–26049

Kokka RP, Vedros NA, Janda JM (1990) Electrophoretic analysis of the surface components of autoagglutinating surface array protein-positive and surface array protein-negative Aeromonas hydrophila and Aeromonas sobria. J Clin Microbiol 28:2240–2247

Koval S, Murray R (1984) The isolation of surface array proteins from bacteria. Can J Biochem Cell Biol 62:1181–1189

Kummer K, Vyalikh D, Blüher A, Sivkov V, Maslyuk V, Bredow T, Mertig I, Mertig M, Molodtsov S (2011) Real-time study of the modification of the peptide bond by atomic calcium. J Phys Chem B 115:2401–2407

Lederer FL, Weinert U, Günther TJ, Raff J, Weiß S, Pollmann K (2013) Identification of multiple putative S-layer genes partly expressed by Lysinibacillus sphaericus JG-B53. Microbiology 159:1097–1108

Lipfert J, Doniach S (2007) Small-angle X-ray scattering from RNA, proteins, and protein complexes. Annu Rev Biophys Biomol Struct 36:307–327

Makhatadze GI, Privalov PL (1995) Energetics of protein structure. Adv Protein Chem 47:307–425

Merroun ML, Raff J, Rossberg A, Hennig C, Reich T, Selenska-Pobell S (2005) Complexation of uranium by cells and S-layer sheets of Bacillus sphaericus JG-A12. Appl Environ Microbiol 71:5532–5543

Pavkov T, Egelseer EM, Tesarz M, Svergun DI, Sleytr UB, Keller W (2008) The structure and binding behavior of the bacterial cell surface layer protein SbsC. Structure 16(8):1226–1237

Peltier J, Courtin P, El Meouche I, Lemee L, Chapot-Chartier MP, Pons JL (2011) Clostridium difficile has an original peptidoglycan structure with a high level of N-acetylglucosamine deacetylation and mainly 3–3 cross-links. J Biol Chem 286:29053–29062

Petoukhov MV, Franke D, Shkumatov AV, Tria G, Kikhney AG, Gajda M, Gorba C, Mertens HD, Konarev PV, Svergun DI (2012) New developments in the program package for small-angle scattering data analysis. J Appl Crystallogr 45:342–350

Pollmann K, Raff J, Schnorpfeil M, Radeva G, Selenska-Pobell S (2005) Novel surface layer protein genes in Bacillus sphaericus associated with unusual insertion elements. Microbiology 151:2961–2973

Prabhu NV, Sharp KA (2005) Heat capacity in proteins. Annu Rev Phys Chem 56:521–548
Privalov PL, Gill SJ (1988) Stability of protein structure and hydrophobic interaction. Adv Protein Chem 39:191–234

Pum D, Sára M, Sleytr U (1989) Structure, surface charge, and self-assembly of the S-layer lattice from Bacillus coagulans E38-66. J Bacteriol 171:5296–5303

Rad B, Haxton T, Shon A, Shin S, Whitelam S, Ajo-Franklin C (2015) Ion-specific control of the self-assembly dynamics of a nanostructured protein lattice. ACS Nano 9:180–190

Raff J, Selenska-Pobell S (2006) Toxic avengers. Nucl Eng Int 51:34–36

Raff J, Soltmann U, Matys S, Selenska-Pobell S, Böttcher H, Pompe W (2003) Biosorption of uranium and copper by biocers. Chem Mater 15:240–244

Rost B, Yachdav G, Liu J (2004) The PredictProtein server. Nucleic Acids Res 32:W321–W326

Roy A, Kucukural A, Zhang Y (2010) I-TASSER: a unified platform for automated protein structure and function prediction. Nat Protoc 5:725–738

Roy A, Yang J, Zhang Y (2012) COFACTOR: an accurate comparative algorithm for structure-based protein function annotation. Nucleic Acids Res 40:W471–W477

Sabet M, Lee S-W, Nauman R, Sims T, Um H-S (2003) The surface (S-) layer is a virulence factor of Bacteroides forsythus. Microbiology 149:3617–3627

Sara M, Sleytr UB (1987) Molecular sieving through S layers of Bacillus stearothermophilus strains. J Bacteriol 169:4092–4098

Sára M, Sleytr UB (2000) S-layer proteins. J Bacteriol 182:859–868

Sarkar SK (1996) NMR spectroscopy and its application to biomedical research. Elsevier Science, Amsterdam

Schuster B, Sleytr UB (2009) Composite S-layer lipid structures. J Struct Biol 168:207–216
Shin A, Chung S, Sanii B, Comollie L, Bertozzi C, De Yoreo J (2012) Direct observation of kinetic traps associated with structural transformations leading to multiple pathways of S-layer assembly. PNAS 109:12968–12973

Sleytr UB (1975) Heterologous reattachment of regular arrays of glycoproteins on bacterial surfaces. Nature Publishing Group, UK

Sleytr U (1978) Regular array of macromolecules on bacterial cell walls: structure, chemistry, assembly, and function. Int Rev Cytol 53:1–64

Sleytr UB, Messner P, Pum D, Sara M (1996) Crystalline bacterial cell surface proteins. Academic, New York

Sleytr UB, Messner P (1983) Crystalline surface layers on bacteria. Annu Rev Microbiol 37:311–339

Sleytr UB, Messner P, Pum D, Sara M (1999) Crystalline bacterial cell surface layers (S layers): from supramolecular cell structure to biomimetics and nanotechnology. Angew Chem Int Ed 38:1034–1054

Sockett RE (2009) Predatory lifestyle of Bdellovibrio bacteriovorus. Annu Rev Microbiol 63:523–539

Svergun D, Barberato C, Koch M (1995) CRYSOL—a program to evaluate X-ray solution scattering of biological macromolecules from atomic coordinates. J Appl Crystallogr 28:768–773

Teixeira L, Strickland A, Mark S, Bergkvist M, Sierra-Sastre Y, Batt C (2010) Entropically driven self-assembly of Lysinibacillus sphaericus S-layer proteins analyzed under various environmental conditions. Macromol Biosci 10:147–155

Valentini E, Kikhney AG, Previtali G, Jeffries CM, Svergun DI (2015) SASBDB, a repository for biological small-angle scattering data. Nucleic Acids Res 43:D357–D363

Weinert U, Pollmann K, Barkleit A, Vogel M, Gunther T, Raff J (2015) Synthesis of S-layer conjugates and evaluation of their modifiability as a tool for the functionalization and patterning of technical surfaces. Molecules 20:9847–9861

Whitmore L, Wallace BA (2008) Protein secondary structure analyses from circular dichroism spectroscopy: methods and reference databases. Biopolymers 89:392–400
Word N, Yousten A, Howard L (1983) Regularly structured and non-regularly structured surface layers of Bacillus sphaericus. FEMS Microbiol Lett 17:277–282

Zhang Y (2008) I-TASSER server for protein 3D structure prediction. BMC Bioinform 9:40